



Microalgal cultures for the remediation of wastewaters with different nitrogen to phosphorus ratios: Process modelling using artificial neural networks

Eva M. Salgado^{a,b,*}, Ana F. Esteves^{a,b,c}, Ana L. Gonçalves^{a,b,d}, José C.M. Pires^{a,b,*}

^a LEPABE – Laboratory for Process Engineering, Environment, Biotechnology and Energy, Faculty of Engineering, University of Porto, Rua Dr. Roberto Frias, 4200-465, Porto, Portugal

^b ALICE – Associate Laboratory in Chemical Engineering, University of Porto, Rua Dr. Roberto Frias, 4200-465, Porto, Portugal

^c LSRE-LCM - Laboratory of Separation and Reaction Engineering - Laboratory of Catalysis and Materials, Faculty of Engineering, University of Porto, Rua Dr. Roberto Frias, 4200-465, Porto, Portugal

^d CITEVE – Technological Centre for the Textile and Clothing Industries of Portugal, Rua Fernando Mesquita, 2785, 4760-034, Vila Nova de Famalicão, Portugal

ARTICLE INFO

Keywords:

Artificial neural network
Chlorella vulgaris
 Genetic algorithms
 Microalgae
 Nutrient removal
 Wastewater treatment

ABSTRACT

Microalgae have remarkable potential for wastewater bioremediation since they can efficiently uptake nitrogen and phosphorus in a sustainable and environmentally friendly treatment system. However, wastewater composition greatly depends on its source and has a significant seasonal variability. This study aimed to evaluate the impact of different N:P molar ratios on the growth of *Chlorella vulgaris* and nutrient removal from synthetic wastewater. Furthermore, artificial neural network (ANN) threshold models, optimised by genetic algorithms (GAs), were used to model biomass productivity (BP) and nitrogen/phosphorus removal rates (RR_N/RR_P). The impact of various inputs culture variables on these parameters was evaluated. Microalgal growth was not nutrient limited since the average biomass productivities and specific growth rates were similar between the experiments. Nutrient removal efficiencies/rates reached $92.0 \pm 0.6\%/6.15 \pm 0.01 \text{ mg}_N \text{ L}^{-1} \text{ d}^{-1}$ for nitrogen and $98.2 \pm 0.2\%/0.92 \pm 0.03 \text{ mg}_P \text{ L}^{-1} \text{ d}^{-1}$ for phosphorus. Low nitrogen concentration limited phosphorus uptake for low N:P ratios (e.g., 2 and 3, yielding $36 \pm 2 \text{ mg}_{DW} \text{ mg}_P^{-1}$ and $39 \pm 3 \text{ mg}_{DW} \text{ mg}_P^{-1}$, respectively), while low phosphorus concentration limited nitrogen uptake with high ratios (e.g., 66 and 67, yielding $9.0 \pm 0.4 \text{ mg}_{DW} \text{ mg}_N^{-1}$ and $8.8 \pm 0.3 \text{ mg}_{DW} \text{ mg}_N^{-1}$, respectively). ANN models showed a high fitting performance, with coefficients of determination of 0.951, 0.800, and 0.793 for BP, RR_N , and RR_P , respectively. In summary, this study demonstrated that microalgae could successfully grow and adapt to N:P molar ratios between 2 and 67, but the nutrient uptake was impacted by these variations, especially for the lowest and highest N:P molar ratios. Furthermore, GA-ANN models demonstrated to be relevant tools for microalgal growth modelling and control. Their high fitting performance in characterising this biological system can contribute to reducing the experimental effort for culture monitoring (human resources and consumables), thus decreasing the costs of microalgal production.

1. Introduction

Microalgae are a diversified group of photosynthetic microorganisms, including eukaryotic microalgae and prokaryotic cyanobacteria (Vale et al., 2020). Compared to many types of plants, microalgae have high growth rates, high photosynthetic efficiency, remarkable adaptability to different environmental conditions and are easy to cultivate

(Escapa et al., 2017; Lv et al., 2017). As a result of all these advantages, these microorganisms have been widely studied for various applications. For instance, due to their rich biomass composition, they can be used for food and feed, and in the pharmaceutical and cosmetic industries (Braun and Colla, 2022; Lucakova et al., 2022). However, one of the most remarkable applications is in wastewater treatment since they can rapidly grow while efficiently removing several contaminants, as well as

* Corresponding authors. ALICE – Associate Laboratory in Chemical Engineering, University of Porto, LEPABE – Laboratory for Process Engineering, Environment, Biotechnology and Energy, Faculty of Engineering, Rua Dr. Roberto Frias, 4200-465, Porto, Portugal.

E-mail addresses: up201606419@fe.up.pt (E.M. Salgado), jcpires@fe.up.pt (J.C.M. Pires).

<https://doi.org/10.1016/j.envres.2023.116076>

Received 28 February 2023; Received in revised form 4 May 2023; Accepted 5 May 2023

Available online 6 May 2023

0013-9351/© 2023 The Authors. Published by Elsevier Inc. This is an open access article under the CC BY-NC-ND license (<http://creativecommons.org/licenses/by-nc-nd/4.0/>).

sequestering CO₂ and generating O₂ (Ahmed et al., 2022; Japar et al., 2021). The possibility of integrating wastewater treatment and CO₂ capture with the production of biofertilisers and bioenergy is another factor that leads to a growing interest in the study of microalgal growth using wastewater as a culture medium. In recent years, several authors have evaluated the treatment of different types of wastewater by growing various microalgal species in municipal (Han et al., 2021; Tran et al., 2020), agricultural (Chen et al., 2020; Ganeshkumara et al., 2018), food processing (Gramegna et al., 2020; Hemalatha et al., 2019) and industrial wastewaters (Behl et al., 2020; Javed et al., 2022; Silva et al., 2021). These wastewaters typically have high concentrations of essential and growth-limiting nutrients for microalgae, such as nitrogen and phosphorus, at various ratios. Nitrogen is a crucial element for regulating algal growth and metabolism, especially for protein synthesis, while phosphorus is essential for the formation of nucleic acids, ATP and the cell membrane (Su, 2021; Umdu, 2020). However, they are conventional pollutants in wastewater and need to be removed before they are released into the water bodies. When effluents are continuously discharged into water courses without proper treatment, increasing the nitrogen and phosphorus concentration in the receiving bodies, harmful algal blooms are formed, leading to the eutrophication phenomenon. In these circumstances, algal blooms produce biotoxins, cause oxygen depletion and contribute to the loss of numerous aquatic species, degrading aquatic ecosystems (Gil-Izquierdo et al., 2021; Suteja et al., 2021). To reduce the risk of this type of event, nitrogen and phosphorus are typically removed from effluents in wastewater treatment plants through biological processes such as aerobic-activated sludge treatments and anaerobic digestion processes followed by nitrification and denitrification (Gonçalves et al., 2017; Li et al., 2019). Nevertheless, traditional biological methods have some limitations such as: (i) limited removal capacity of inorganic nutrients and micropollutants; (ii) the necessity of various cycles, tanks, and internal recycling of activated sludge, which results in high costs and energy requirements; and (iii) loss of potentially valuable nutrients (Chai et al., 2021; Gonçalves et al., 2017). Microalgal treatment systems can be more efficient, sustainable, and environmentally friendly, requiring lower capital investment and operation costs and providing natural disinfection and valuable microalgal biomass, which balances the energetic requirements for microalgal cultivation (Leong et al., 2022; Mohsenpour et al., 2021; Sutherland and Ralph, 2019).

Wastewaters present a widely variable composition, depending on the type, location, and season. Hence, wastewater treatment systems, particularly biological ones, entail complex non-linear dynamics due to the large variations in the influent, which can make it difficult to operate them and comply with rigorous environmental legislation. Therefore, it is crucial to improve the performance of current wastewater treatment systems as well as employ efficient process control strategies (Bahramian et al., 2023; Wang et al., 2022). Mathematical models based on artificial intelligence and soft-computing have been increasingly studied throughout the years as tools to predict, control and/or optimise process variables. Artificial Neural Networks (ANNs) are a popular machine-learning technique that mimic the interaction between neurons and the learning process in the human brain (Jawad et al., 2021). These models have been gaining increased attention throughout the years and have prevailed over other tools, such as support vector machines, decision trees, and fuzzy logic, in recent wastewater treatment modelling studies (Bahramian et al., 2023). In this technique, a representative dataset of input and output variables is used to train the network, which allows an efficient description of non-linear interactions and patterns between different process variables with a high fitting performance (Sakiewicz et al., 2020). Feedforward ANNs are common network types in which the information flows through synapses or weights in only one direction: from the artificial neurons in an input layer through a hidden layer towards an output layer, using an activation function (Zhang et al., 2019). ANNs have been widely used to model biological wastewater treatment systems such as activated sludge processes (Fard et al., 2020;

Jana et al., 2022; Moral et al., 2008). However, few studies report the use of these networks to model microalgal wastewater bioremediation, particularly nitrogen and phosphorus removal. To the best of the authors' knowledge, Arranz et al. (2008) presented the first study in which ANNs were applied to describe an algae-based treatment by predicting salicylate biodegradation by an algal-bacterial consortium. Parameters such as light intensity, hydraulic retention time, temperature, and salicylate concentration were tested as input variables. The authors observed a high fitting performance of the ANN model with a coefficient of determination (R^2) of 0.999. Recently, Carvalho et al. (2021) used ANNs to model microalgal tertiary treatment of a domestic effluent retrieved from an upflow anaerobic sludge blanket, aiming to predict ammonium and phosphate removal. Variables such as light intensity, initial concentration of ammonium and phosphate ions, and initial biomass concentration were used as input variables. The model presented a high fitting (R^2 over 0.950) for both outputs (ammonium and phosphorus concentration), indicating that ANNs can be a great tool for predicting microalgal wastewater treatment. However, existing studies on the use of ANNs to describe nitrogen and phosphorus removal typically only consider pollutant removal efficiencies and not kinetic removal parameters. Furthermore, ANNs require a robust dataset. The number of experimental points should be higher than the number of model parameters (weights) (Liyanaarachchi et al., 2020), usually not contemplated in these studies. Another difficulty is the optimisation of the ANN hyperparameters, as it requires the definition of certain parameters, such as the input variables, number of hidden layers and neurons, and activation functions (Afonso and Pires, 2017). Genetic algorithms (GAs) are evolutionary algorithms which can be a great tool to optimise these parameters. In a nutshell, these algorithms are based on Darwin's evolution theory, in which a population of chromosomes is generated and suffers selection, mutation, and crossover through various generations. This process allows to obtain the fittest chromosomes, containing information regarding the optimised solution (Katoch et al., 2021; Mirjalili et al., 2020).

For microalgae-based treatment systems that aim to combine biomass production and wastewater treatment, it is essential to understand and predict how variations in nitrogen and phosphorus concentrations can impact microalgal growth and the removal of these pollutants. Therefore, the main objectives of this work were: (i) to evaluate the effect of a wide range of nitrogen to phosphorus (N:P) molar ratios in a synthetic effluent on the growth of the microalga *Chlorella vulgaris* and nitrogen and phosphorus removal; (ii) to develop effective threshold models with ANNs, with a structure defined by GAs, to describe biomass productivities and nutrient removal rates based on the cultivation time and the initial and/or instantaneous concentrations of biomass and nutrients; and (iii) to determine the key process variables and their impact on biomass productivity and nutrient removal.

2. Materials and methods

2.1. Inoculum preparation

The microalgal strain *C. vulgaris* CCAP 211/11 B was obtained from the Culture Collection of Algae and Protozoa, CCAP, United Kingdom. Stock cultures were maintained in 100-mL flasks at room temperature in a modified OECD (Organisation for Economic Cooperation and Development) test medium. The culture medium was prepared as follows: 500 mg NaHCO₃, 250 mg NaNO₃; 45 mg KH₂PO₄; 18 mg CaCl₂·2H₂O; 15 mg MgSO₄·7H₂O; 12 mg MgCl₂·6H₂O; 415 µg MnCl₂·4H₂O; 185 µg H₃BO₃; 100 µg Na₂EDTA·2H₂O; 80 µg FeCl₃·6H₂O; 7 µg Na₂MoO₄·2H₂O; 3 µg ZnCl₂; 1.5 µg CoCl₂·6H₂O; and 0.01 µg CuCl₂·2H₂O per liter. Microalgae were supplied with a light intensity of 6.5 µmol m⁻² s⁻¹, measured using a Delta OHM HD2102.2 portable photo/radiometer, under light:dark cycle of 24:0 h. Constant agitation at 120 rotations per minute (rpm) was provided by an Unimax 1010 orbital shaker (Heidolph, Germany).

2.2. Experimental setup

C. vulgaris was cultured in 5-L photobioreactors (PBRs) operating in batch mode for 9–11 d, with an average light intensity of $558 \mu\text{mol m}^{-2} \text{s}^{-1}$, supplied continuously by a light-emitting diode (LED) panel, as represented in the experimental setup in Fig. 1. Synthetic wastewater was used as the culture medium, by altering the nitrate-nitrogen ($\text{NO}_3\text{-N}$) and phosphate-phosphorus ($\text{PO}_4\text{-P}$) concentrations in the OECD test medium to simulate the use of real wastewaters. Fifteen different assays were conducted with N:P molar ratios ranging between 2 and 67 (Table 1) to include values reported in the literature for various types of real wastewaters used to culture microalgae (Gramegna et al., 2020; Silva et al., 2021; Tao et al., 2017; Tran et al., 2020). Experiments were conducted with an average initial biomass concentration in terms of dry weight (DW) of $29 \pm 1 \text{ mg}_{\text{DW}} \text{ L}^{-1}$. Filtered atmospheric air ($0.2\text{-}\mu\text{m}$ cellulose acetate membranes, Orange Scientific, Braine-l'Alleud, Belgium) was supplied to the cultures at 1.5 L min^{-1} to promote agitation and CO_2 supplementation using AP-180 air pumps (Trixie, Flensburg, Germany). A Consort's C6010 electrochemical analyser (Brussels, Belgium) was used to monitor the temperature and pH daily, and the latter was adjusted daily to approximately 7 using a 10% (v/v) HCl solution.

2.3. Growth monitoring

Microalgal growth was monitored daily by measuring the culture's optical density (OD) at 680 nm in duplicate with a V-530 UV/VIS spectrophotometer (Jasco, Tokyo, Japan). The OD was plotted against the biomass concentration in $\text{mg}_{\text{DW}} \text{ L}^{-1}$ to build a calibration curve. The biomass concentration was determined according to a standard method described in APHA (2017): 10 mL culture samples were placed in previously weighed porcelain crucibles and dried at $105 \text{ }^\circ\text{C}$ for 24 h. After drying, the crucibles were weighed, and the biomass concentration was obtained based on the weight difference per sample volume.

Certain growth parameters were calculated based on the biomass concentration over time to compare the microalgal growth between experiments. The specific growth rate (μ , d^{-1}) was determined according to Eq. (1), in which X_1 and X_2 correspond to the biomass concentration in $\text{mg}_{\text{DW}} \text{ L}^{-1}$, at the beginning (t_1 , d) and at the end (t_2 , d) of the exponential growth phase, respectively. The average biomass productivity (BP_{avg} , $\text{mg}_{\text{DW}} \text{ L}^{-1} \text{ d}^{-1}$) was determined according to Eq. (2), where X_0 and X_f ($\text{mg}_{\text{DW}} \text{ L}^{-1}$) correspond to the biomass concentration at the beginning (t_0 , d) and at the end (t_f , d) of the experiment, respectively. Biomass productivities (BP , $\text{mg}_{\text{DW}} \text{ L}^{-1} \text{ d}^{-1}$) were calculated between every two consecutive experimental points (Eq. (3)): biomass concentration, X_{y+1} ($\text{mg}_{\text{DW}} \text{ L}^{-1}$), at time t_{y+1} (d) and biomass concentration, X_y ($\text{mg}_{\text{DW}} \text{ L}^{-1}$), at time t_y (d).

$$\mu = \frac{\ln(X_2/X_1)}{(t_2 - t_1)} \quad (1)$$

Table 1

Nitrogen and phosphorus concentrations in the synthetic wastewater at the beginning of each experiment.

Assay	Initial N:P molar ratios	N_0 ($\text{mg}_\text{N} \text{ L}^{-1}$)	P_0 ($\text{mg}_\text{P} \text{ L}^{-1}$)
1	2	9.7 ± 0.2	8.6 ± 0.2
2	3	9.7 ± 0.2	8.4 ± 0.3
3	5	20 ± 1	8.5 ± 0.2
4	7	26 ± 2	8.7 ± 0.2
5	8	39.8 ± 0.1	10.54 ± 0.07
6	9	40.5 ± 0.4	10.1 ± 0.6
7	14	66.0 ± 0.4	10.2 ± 0.6
8	19	94.5 ± 0.7	10.8 ± 0.5
9	28	98.0 ± 0.4	7.7 ± 0.5
10	41	103.4 ± 0.1	5.6 ± 0.3
11	43	98.2 ± 0.1	5.1 ± 0.2
12	52	103.1 ± 0.1	4.4 ± 0.5
13	59	84.9 ± 0.1	3.19 ± 0.02
14	66	91.6 ± 0.7	3.06 ± 0.07
15	67	94 ± 2	3.11 ± 0.08

N_0 : initial nitrogen concentration; P_0 : initial phosphorus concentration.

$$BP_{\text{avg}} = \frac{X_f - X_0}{t_f - t_0} \quad (2)$$

$$BP_y = \frac{X_{y+1} - X_y}{t_{y+1} - t_y} \quad (3)$$

2.4. Removal of nitrogen and phosphorus

The nitrogen and phosphorus concentrations were monitored over time in each assay. $\text{NO}_3\text{-N}$ concentration was determined in triplicate by filtering a diluted sample through $0.2\text{-}\mu\text{m}$ cellulose acetate membranes and measuring the OD at 220 nm in a T80 UV/VIS Spectrophotometer (PG Instruments, United Kingdom), as described by Gonçalves et al. (2016). A calibration curve was prepared using NaNO_3 standard solutions and following the same procedure. $\text{PO}_4\text{-P}$ concentration was evaluated in triplicate using the ammonium molybdate colourimetric method described by Lee et al. (2009). This method is based on the reaction between inorganic phosphate and ammonium molybdate in the presence of a reducing agent (ascorbic acid) and the OD measurement of the phosphomolybdate complex at 820 nm. KH_2PO_4 standard solutions were used to build the calibration curve.

To evaluate nutrient removal, parameters such as nitrogen and phosphorus mass removal (MR , mg L^{-1}), removal efficiency (RE , %) and average removal rate (RR_{avg} , $\text{mg L}^{-1} \text{ d}^{-1}$) were determined as described in Eqs. (4)–(6), respectively. In these equations, S_0 (mg L^{-1}) represents the nutrient concentration at the beginning of the experiment (t_0) and S_f (mg L^{-1}) at the end (t_f). Removal rates were determined between every two consecutive experimental points as presented in Eq. (7), where S_{y+1} (mg L^{-1}) corresponds to the nutrient concentration at time t_{y+1} , and S_y (mg L^{-1}) to the nutrient concentration at time t_y .

$$MR = S_0 - S_f \quad (4)$$

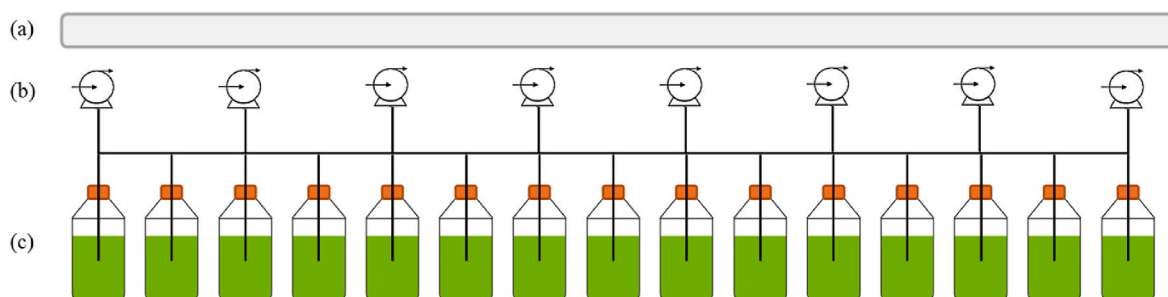


Fig. 1. Experimental setup: (a) light source (LED panel); (b) atmospheric air pumps; (c) photobioreactors.

$$RE = \frac{S_0 - S_f}{S_0} \times 100 \quad (5)$$

$$RR_{avg} = \frac{S_0 - S_f}{S_0} \quad (6)$$

$$RR_y = \frac{S_{y+1} - S_y}{t_{y+1} - t_y} \quad (7)$$

A modified Gompertz model was applied to describe the variation of nitrogen and phosphorus concentrations over time, as presented in Eq. (8). The nutrient uptake rate is presented as k in d^{-1} and the lag time as λ in d . The Solver supplement of Microsoft Excel V. 2301 was used to minimise the sum of squared residuals and determine k and λ . The R^2 and root mean squared error, $RMSE$, were calculated as presented in Eqs. (9) and (10), to assess the fitting performance of the models. In these equations, z represents the experimental nutrient concentrations, \hat{z}_i corresponds to the concentrations predicted by the model, and \bar{z} to the average concentrations of n samples.

$$S(t) = S_i + (S_f - S_i) \times \exp[-\exp(k(\lambda - t) + 1)] \quad (8)$$

$$R^2 = 1 - \frac{\sum_{i=1}^n (z_i - \hat{z}_i)^2}{\sum_{i=1}^n (z_i - \bar{z})^2} \quad (9)$$

$$RMSE = \sqrt{\frac{\sum_{i=1}^n (z_i - \hat{z}_i)^2}{n}} \quad (10)$$

Moreover, the biomass yield as a function of nitrogen/phosphorus consumption ($Y_{X/S}$) was calculated according to Eq. (11).

$$Y_{X/S} = \frac{X_f - X_0}{S_0 - S_f} \quad (11)$$

2.6. Statistical analysis

Average values and standard deviation were determined for each parameter. The differences between the calculated parameters from each experiment were evaluated through a one-way analysis of variance (ANOVA) with Tukey's multi-comparison test at a significance level of 0.05, using GraphPad Prism V. 8.0. Prior to the ANOVA analysis, a Shapiro-Wilk test of normality was conducted to verify the normal distribution of the data.

2.7. Development of the GA-ANN models

Feedforward threshold ANNs were developed to describe BP and nitrogen (RR_N)/phosphorus (RR_P) removal rates based on the time of cultivation and the initial and/or instantaneous concentrations of

biomass and nutrients. Threshold models were used in this study since BP , RR_N , and RR_P (output variables) present two different behaviour regimes, depending on the value of a certain input variable (threshold). For instance, BP can be divided into two regimes as a result of different microalgal growth phases, while nutrient removal rates can heavily depend on the nutrient concentrations. Each model was constructed as presented in Eq. (12), in which y corresponds to the output, ANN_1 and ANN_2 represent the networks for each regime, x_i are the input variables, and x_d and r are the threshold variable and value, respectively.

$$y = \begin{cases} ANN_1(x_i), & \text{if } x_d \leq r \\ ANN_2(x_i), & \text{if } x_d > r \end{cases} \quad (12)$$

The networks were divided into three layers: input, hidden and output. Fig. 2 shows a generalised schematic representation of the ANNs constructed in the present work. Eight different input or explanatory variables were tested for each ANN: initial ($N:P_0$) and instantaneous ($N:P_i$) N:P ratio, initial (N_0) and instantaneous (N_i) nitrogen concentration, initial (P_0) and instantaneous (P_i) phosphorus concentration, time of cultivation (t), and instantaneous biomass concentration (X_i). GAs were used to define the optimal structure of ANN threshold models, as described by Afonso and Pires (2017). For each model, the fittest chromosome (corresponding to the lowest $RMSE$ values – fitness function, and not considering the ones with the number of model parameters higher than the number of experimental points) contained information regarding the threshold variable, threshold value, type of activation function, number of neurons in the hidden layer (hidden neurons), and chosen input variables. The models were determined with the following specifications: (i) population size of 100; (ii) selection probability of 0.20; (iii) selection criterion based on elitism; (iv) crossover probability of 0.70; (v) mutation probability of 0.1; (vi) evaluation of $RMSE$ in training and validation sets; and (vii) a stopping criterion based on the maximum number of generations. The activation function for the output layer was deemed linear, while for the hidden layer, GAs selected non-linear functions such as the hyperbolic tangent sigmoid (tansig), radial basis (radbas), logarithmic sigmoid (logsig) or inverse transfer function (netinv). The dataset was composed of 125 experimental points and divided into 75% training and 25% validation. The training process was stopped once there was an increase in the error during validation (early stopping method), avoiding overfitting. The predicted outputs were plotted against the experimental data, and the fitting performance of the statistical model was evaluated based on R^2 and $RMSE$. Moreover, 2D contour and 3D surface plots were built to evaluate the combined effect of input variables on the outputs. In these diagrams, the interaction of the output variable with two input variables (in the range of the experimental data) was assessed, while the rest were fixed as the median of the values. MATLAB® software (R2016a, MathWorks, USA, 2016) was used for the tasks described throughout this section.

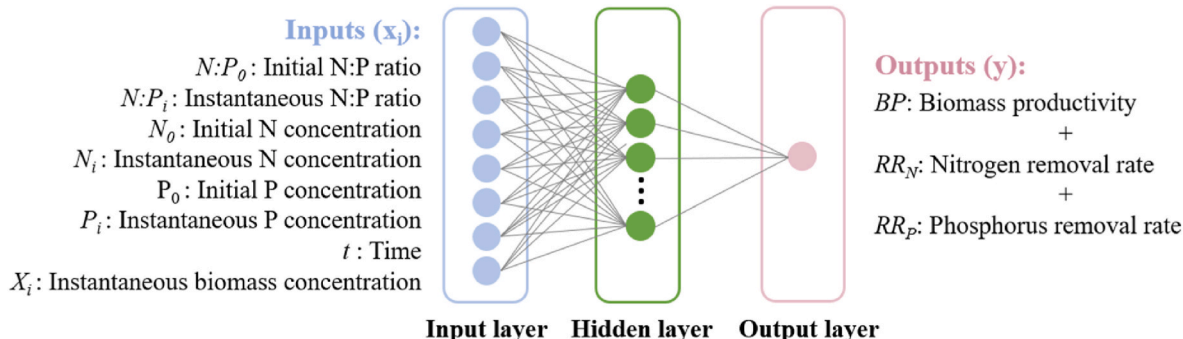


Fig. 2. Generic schematic representation of the ANNs developed in the present work.

3. Results and discussion

3.1. *Chlorella vulgaris* growth with different N:P ratios

C. vulgaris grew successfully in all experimental conditions with an overall similar growth behaviour. No lag phase was observed in any of the experiments. The exponential growth phase lasted until day 3 of cultivation, after which a decline in the exponential microalgal growth and the beginning of the stationary phase was observed. Fig. 3 presents the growth parameters determined for each experiment. The X_{\max} values (Fig. 3A) varied between $203 \pm 14 \text{ mg}_{\text{DW}} \text{ L}^{-1}$ for ratio 2 and $285 \pm 6 \text{ mg}_{\text{DW}} \text{ L}^{-1}$ for ratio 8. However, X_{\max} was significantly lower ($p < 0.05$) for ratios 2 and 3 compared to the remaining assays. In terms of biomass productivity (Fig. 3C), the lowest BP_{avg} value ($20 \pm 2 \text{ mg}_{\text{DW}} \text{ L}^{-1} \text{ d}^{-1}$) was obtained for ratio 2 and the highest ($24.7 \pm 0.1 \text{ mg}_{\text{DW}} \text{ L}^{-1} \text{ d}^{-1}$) for ratio 52. However, the average value for ratio 2 was not statistically different ($p > 0.05$) from ratios 3, 14, 19 and 66, which indicates that nitrogen concentration did not impact the BP_{avg} . Moreover, even though the maximum value was observed for ratio 52, it was only statistically different ($p < 0.05$) from the values obtained for ratios 2, 3 and 19. The specific growth rates (Fig. 3B) ranged between $0.54 \pm 0.03 \text{ d}^{-1}$ and $0.588 \pm 0.008 \text{ d}^{-1}$, corresponding to ratios 8 and 52, respectively. Comparing the different N:P ratios, the μ values did not largely vary between experiments and even though significant in some cases, only slight differences were observed between the average values. For instance, ratio 52 provided higher μ compared to ratios 2–14, 28–43, 66, and 67 ($p < 0.05$), but was not statistically different from ratios 19 and 59 ($p > 0.05$). Therefore, the initial nutrient concentration does not appear to have severely impacted microalgal growth during the

exponential growth phase. Similar results were obtained by Chu et al. (2022) when testing the growth of the same microalgal species in reused synthetic wastewater supplemented with different $\text{NO}_3\text{-N}$ and $\text{PO}_4\text{-P}$ concentrations: $31.5\text{--}280.3 \text{ mg}_\text{N} \text{ L}^{-1}$ and $1.2\text{--}28.7 \text{ mg}_\text{P} \text{ L}^{-1}$. The specific growth rates were not statistically different between N:P molar ratios of 2, 7, 13, 20, 22 and 663, ranging between 0.55 ± 0.01 and $0.59 \pm 0.03 \text{ d}^{-1}$. Furthermore, Silva et al. (2015) evaluated the growth of *C. vulgaris* in OECD test medium with a $\text{PO}_4\text{-P}$ concentration of $4.6 \text{ mg}_\text{P} \text{ L}^{-1}$ and $\text{NO}_3\text{-N}$ concentrations of 16, 33, and $49 \text{ mg}_\text{N} \text{ L}^{-1}$, corresponding to N:P molar ratios of 8, 16 and 24. The authors also obtained similar μ values regardless of the N:P ratio: 0.66 ± 0.03 , 0.67 ± 0.04 , and $0.61 \pm 0.03 \text{ d}^{-1}$ for ratios 8, 16 and 24, respectively. Compared to the present study, the slightly higher specific growth rates obtained by Silva et al. (2015) might be justified by different experimental conditions, such as light source and intensity supplied to the cultures.

The similar growth parameters between the assays suggest that in the experimental conditions of the present study, nitrogen and phosphorus concentrations did not significantly impact microalgal growth. In response to variations in their environment, such as changes in the nutrient ratios, microalgae can remain in homeostasis, maintaining the biomass composition and functional activities while sacrificing their growth, or adjust their metabolic fluxes and resource utilisation to adapt to these new conditions (Fernandes et al., 2020). For instance, under limiting phosphorus concentrations, microalgae can shift their metabolic pathways towards the accumulation of energy-rich macromolecules, such as lipids, while maintaining their regular growth (Yaakob et al., 2021). Hence, in the present study, *C. vulgaris* most likely altered its flux rates, particularly nutrient consumption fluxes, in response to the different nitrogen and phosphorus concentrations, being able to

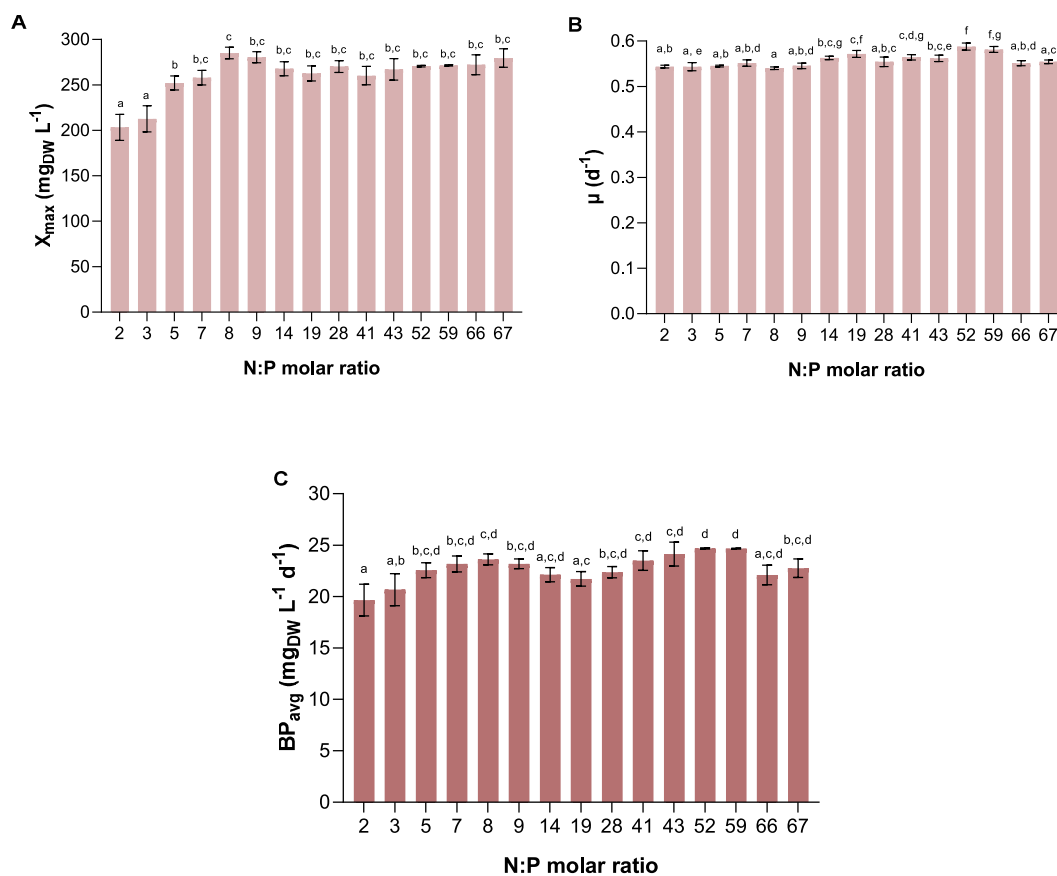


Fig. 3. Variation of the maximum biomass concentration, X_{\max} (A), specific growth rate, μ (B), and average biomass productivity, BP_{avg} (C), with different initial N:P molar ratios. Each column corresponds to the mean value of 3 samples, and error bars represent the standard deviation. For each parameter, values sharing at least one common letter (a, b, c, d, e, f, and g) are not statistically different ($p > 0.05$).

maintain a constant growth pattern. Therefore, it is crucial to evaluate nutrient removal in each experiment, as presented in Section 3.2. To observe growth limitation, possibly lower nitrogen or phosphorus concentrations would have to be tested. Nevertheless, these results demonstrate that this microalgal strain easily adapts to different culture medium compositions, which is useful when working with real wastewater.

3.2. Nutrient removal

For microalgae-based wastewater treatment systems, evaluating how the different influent nutrient loads impact their ability to remove them from the wastewaters is essential. Fig. 4 presents the nitrogen removal parameters obtained for each experiment. The removal efficiency (Fig. 4 C) was generally higher for lower ratios and consequently lower initial nitrogen concentrations (Fig. 4 A) compared to the higher ratios, as

there was less nitrogen available to be consumed by microalgae. The highest values were observed for ratios 2–9, ranging from $74.8 \pm 0.3\%$ for ratio 8 to $92.0 \pm 0.6\%$ for ratio 7. As the ratios increased along with the initial nitrogen concentration, the removal efficiencies generally decreased since microalgae could not uptake all the available nitrogen. The lowest values, $29 \pm 3\%$ and $30 \pm 2\%$ were observed for ratios 66 and 67, respectively. From ratios 2 to 41, the increase in the initial nitrogen concentration reflected an increase in the mass removal (Fig. 4 B) and average removal rate (Fig. 4 D), with values ranging from $7.6 \pm 0.2 \text{ mg}_N \text{ L}^{-1}$ to $60.8 \pm 0.1 \text{ mg}_N \text{ L}^{-1}$ and from $0.86 \pm 0.03 \text{ mg}_N \text{ L}^{-1} \text{ d}^{-1}$ to $6.15 \pm 0.01 \text{ mg}_N \text{ L}^{-1} \text{ d}^{-1}$, respectively. However, comparing higher ratios such as 66 and 67 with lower ratios such as 19, approximately 40% lower nitrogen removal rates ($p < 0.05$) can be observed, for similar initial nitrogen concentrations. In the experiments with the highest N:P ratios, phosphorus appears to be the limiting element since it was present at lower concentrations. Therefore, these results suggest that

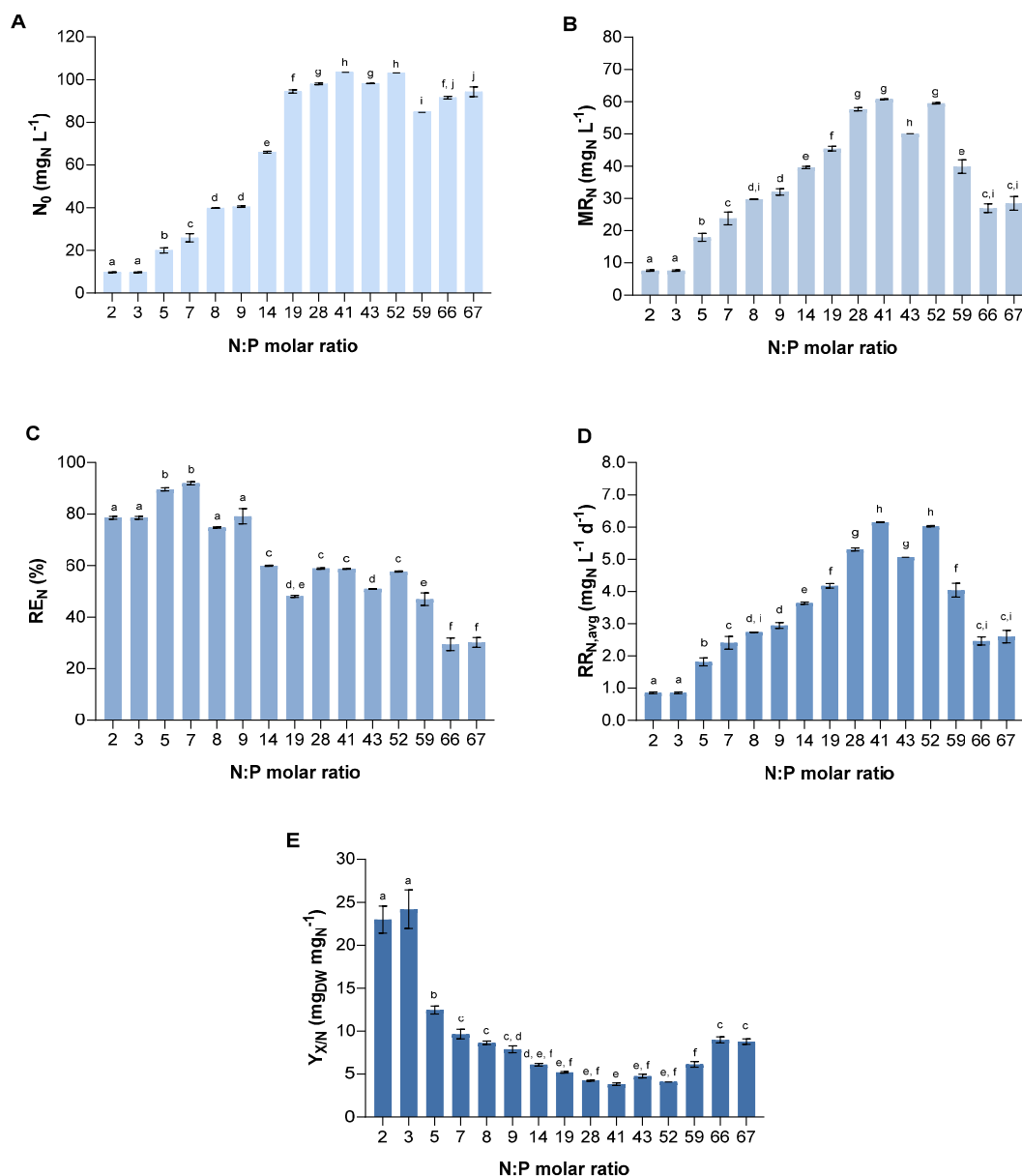


Fig. 4. Variation of the initial nitrogen concentration, N_0 (A), nitrogen mass removal, MR_N (B), nitrogen removal efficiency, RE_N (C), average nitrogen removal rate, $RR_{N,avg}$ (D), and biomass yield in function of nitrogen consumption, $Y_{X/N}$ (E), with different initial N:P molar ratios. Each column corresponds to the mean value of 3 samples, and error bars represent the standard deviation. For each parameter, values sharing at least one common letter (a, b, c, d, e, f, g, h, i and j) are not statistically different ($p > 0.05$).

phosphorus concentration limited the nitrogen uptake for high N:P ratios. Regarding the biomass yield in terms of nitrogen consumption (Fig. 4 E), the highest values ($p < 0.05$) were observed for ratios 2 and 3 ($23 \pm 2 \text{ mg}_{\text{DW}} \text{ mg}_{\text{N}}^{-1}$ and $24 \pm 2 \text{ mg}_{\text{DW}} \text{ mg}_{\text{N}}^{-1}$, respectively). These results indicate that *C. vulgaris* accumulated less nitrogen to produce the same amount of biomass and reflect a very low nitrogen content in the biomass (approximately 4% m/m) due to the low availability of this nutrient in the synthetic wastewater. The lowest values were observed for ratios 14–59, between $3.8 \pm 0.2 \text{ mg}_{\text{DW}} \text{ mg}_{\text{N}}^{-1}$ and $6.1 \pm 0.3 \text{ mg}_{\text{DW}} \text{ mg}_{\text{N}}^{-1}$, which correspond to nitrogen contents of 16%–26% (m/m). Various authors have evaluated the elemental composition of *Chlorella vulgaris* biomass and reported nitrogen contents between 7.0 and 15% (m/m) (Cordoba-Perez and Lasa, 2021; Kröger et al., 2018; Raheem et al., 2015). Comparing ratio 19 with 66 and 67, for similar initial nitrogen concentrations, $Y_{X/N}$ was significantly higher in the latter ($p <$

0.05): $9.0 \pm 0.4 \text{ mg}_{\text{DW}} \text{ mg}_{\text{N}}^{-1}$ and $8.8 \pm 0.3 \text{ mg}_{\text{DW}} \text{ mg}_{\text{N}}^{-1}$, respectively. Therefore, phosphorus limitation resulted in lower nitrogen content in the biomass.

Overall, *C. vulgaris* efficiently removed phosphorus from the synthetic wastewater. The phosphorus removal parameters for each ratio are presented in Fig. 5. The removal efficiencies (Fig. 5 C) were not statistically different ($p > 0.05$) between ratios 8–67 and reached values up to 98%. The lowest values, $56 \pm 2\%$ and $56 \pm 1\%$, were observed for the smallest ratios, 2 and 3, respectively, since they represented the highest initial phosphorus concentrations (Fig. 5 A). As the initial concentrations decreased from ratios 19 to 67, a decrease in the mass removal (Fig. 5 B) and removal rates (Fig. 5 D) was also observed. These removal parameters varied between $2.90 \pm 0.07 \text{ mg}_{\text{P}} \text{ L}^{-1}/0.264 \pm 0.006 \text{ mg}_{\text{P}} \text{ L}^{-1} \text{ d}^{-1}$ for ratio 66 and $10.0 \pm 0.3 \text{ mg}_{\text{P}} \text{ L}^{-1}/0.92 \pm 0.03 \text{ mg}_{\text{P}} \text{ L}^{-1} \text{ d}^{-1}$ for ratio 19. Comparing ratios 5 and 7 with ratios 2 and 3, for

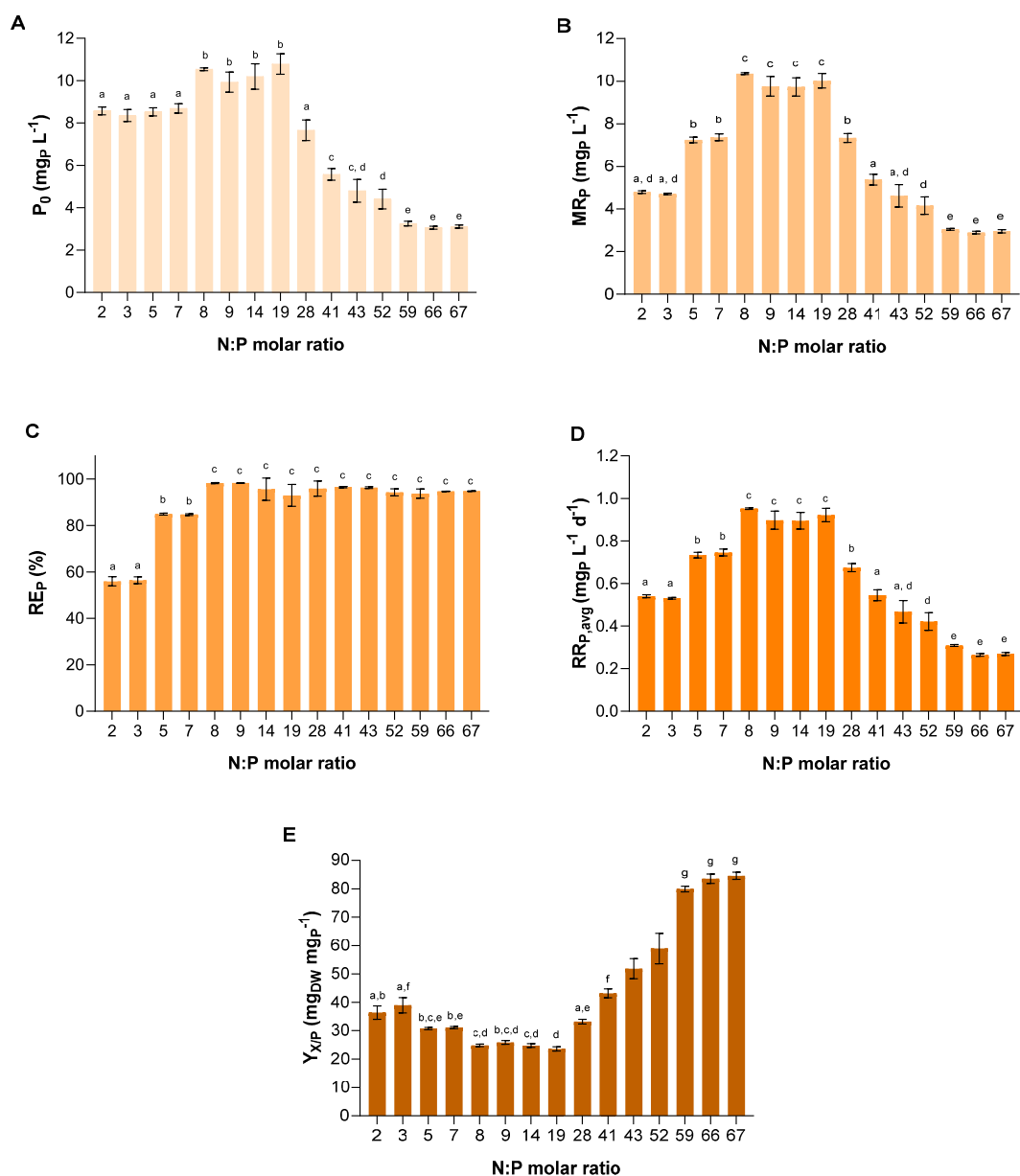


Fig. 5. Variation of the initial phosphorus concentration, P_0 (A), phosphorus mass removal, MR_P (B), phosphorus removal efficiency, RE_P (C), average phosphorus removal rate, $RR_{P,avg}$ (D), and biomass yield in function of phosphorus consumption, $Y_{X/P}$ (E), with different initial N:P molar ratios. Each column corresponds to the mean value of 3 samples, and error bars represent the standard deviation. For each parameter, values sharing at least one common letter (a, b, c, d, e, f, and g) are not statistically different ($p > 0.05$).

similar initial phosphorus concentrations, the removal rates were approximately 28% lower ($p < 0.05$) for the latter. Therefore, the lower initial nitrogen concentrations led to a decrease in phosphorus uptake. Hence, nitrogen concentration appears to be a limiting factor for phosphorus removal. The same tendency was observed in the biomass yield in terms of phosphorus uptake (Fig. 5 E), as higher values ($p < 0.05$) were observed for ratios 2 and 3 ($36 \pm 2 \text{ mg}_{\text{DW}} \text{ mg}_{\text{P}}^{-1}$ and $39 \pm 3 \text{ mg}_{\text{DW}} \text{ mg}_{\text{P}}^{-1}$, respectively) compared to 5 and 7 ($30.8 \pm 0.4 \text{ mg}_{\text{DW}} \text{ mg}_{\text{P}}^{-1}$ and $31.1 \pm 0.4 \text{ mg}_{\text{DW}} \text{ mg}_{\text{P}}^{-1}$, respectively), reflecting a lower phosphorus content in the biomass for lower initial nitrogen concentrations (approximately 3% m/m). The highest values, $84 \pm 2 \text{ mg}_{\text{DW}} \text{ mg}_{\text{P}}^{-1}$ and $85 \pm 1 \text{ mg}_{\text{DW}} \text{ mg}_{\text{P}}^{-1}$, corresponded to the experiments with the lowest initial phosphorus concentrations (ratios 66 and 67, respectively), resulting in an approximate phosphorus content of 1% (m/m) in the microalgal biomass. The Redfield N:P ratio of 16:1 is usually presented as the optimal ratio in microalgal biomass, suggesting that they typically accumulate more nitrogen than phosphorus (Hossain et al., 2022; Li et al., 2022). In fact, according to the molecular formula for microalgal biomass ($\text{C}_{106}\text{H}_{263}\text{O}_{110}\text{N}_{16}\text{P}$), the nitrogen and phosphorus contents are approximately 6.3% (m/m) and 0.9% (m/m), respectively (Salgado and Pires, 2023). This is in accordance with the overall higher $Y_{X/P}$ values compared to $Y_{X/N}$ and, consequently, lower phosphorus content in the biomass. Nevertheless, as evidenced in this study, the same microalgal strain can present different nutrient removal patterns depending on the environmental conditions in which they are cultivated, which can cause variations in the accumulated N:P ratio in the microalgal biomass.

In summary, these results indicate that with low N:P ratios, such as 2 and 3, nitrogen can limit phosphorus uptake by microalgae, while phosphorus might limit nitrogen uptake with high ratios, such as 66 and 67. The absence or shortage of nitrogen can impact the synthesis of proteins required for phosphorus uptake and for overall cellular metabolism (Whitton et al., 2015). On the other hand, ATP synthesis can be jeopardised due to phosphorus limitation, which in turn can impact the entire cellular metabolism, including nitrogen uptake requirements.

Various studies have reported the impact of different nitrogen and phosphorus concentrations on *C. vulgaris* nutrient uptake. Choi and Lee (2015) tested the effect of N:P molar ratios between 2 and 176 in municipal wastewater on the growth and nutrient removal ability of *C. vulgaris*. The authors observed that phosphorus removal greatly depended on its intracellular concentration, the N:P ratio, and the microalgal physiological state. Furthermore, the authors concluded that higher N:P ratios led to higher cellular nitrogen content and lower phosphorus content. The optimal N:P ratios for biomass productivity and nutrient removal efficiencies were between 11 and 66. Cheng et al. (2017) used different initial $\text{PO}_4\text{-P}$ ($2\text{--}10 \text{ mg}_{\text{P}} \text{ L}^{-1}$) and ammonium-nitrogen ($\text{NH}_4\text{-N}$, $10\text{--}50 \text{ mg}_{\text{N}} \text{ L}^{-1}$) concentrations in Bold's

Basal medium to simulate the bioremediation of an anaerobic secondary effluent with *C. vulgaris*. The authors observed a limitation in nitrogen removal for initial phosphorus concentrations below $4 \text{ mg}_{\text{P}} \text{ L}^{-1}$. Alkete et al. (2017) tested N:P molar ratios between 0.68 and 128 for a *C. vulgaris* culture in MLA culture medium, with initial nitrogen and phosphorus concentrations of $0\text{--}56 \text{ mg}_{\text{N}} \text{ L}^{-1}$ and $0\text{--}19 \text{ mg}_{\text{P}} \text{ L}^{-1}$, respectively. The authors observed that N:P molar ratios higher than 57 indicated phosphorus limitation in terms of growth and nutrient removal efficiencies, while ratios lower than 8 reflected nitrogen limitation. By evaluating the specific growth rates, average biomass productivities and nutrient removal efficiencies, the authors concluded that $70 \text{ mg}_{\text{N}} \text{ L}^{-1}$ and $7 \text{ mg}_{\text{P}} \text{ L}^{-1}$ (N:P molar ratio of 22) were the optimal nutrient concentrations. However, these studies do not consider other nutrient removal parameters besides the removal efficiency.

In the present study, besides analysing the removal parameters determined between the beginning and end of the experiments, Gompertz models were applied to the experimental nitrogen and phosphorus concentrations over time. The Gompertz model kinetic parameters are presented in Table 2. The model was generally effectively fitted to the experimental data and characterised by high R^2 and low RMSE values. However, the nitrogen model for ratio 67 had the lowest fitting performance; hence the removal parameters presented in Table 2 were not considered when comparing the different experiments. For certain N:P ratios, a clear lag phase was initially observed, for both nitrogen and phosphorus. However, due to the high standard deviations, no statistical differences were observed between the lag time values ($p > 0.05$). Comparing the nitrogen uptake rates, lower ratios such as 2, 3 and 14 resulted in significantly higher ($p < 0.05$) values compared to the remaining experiments: $1.4 \pm 0.8 \text{ d}^{-1}$, $1.5 \pm 0.1 \text{ d}^{-1}$, and $1.1 \pm 0.2 \text{ d}^{-1}$, respectively. Therefore, nitrogen appears to have been consumed faster for lower initial nitrogen concentrations. On the other hand, ratios 66 and 67 led to the highest phosphorus uptake rates ($p < 0.05$), while the remaining values were not statistically different between themselves ($p > 0.05$). These results indicate that microalgae consumed this nutrient much faster for lower initial available phosphorus. Salgado et al. (2022) also observed a higher phosphorus uptake rate when growing *C. vulgaris* in a secondary urban effluent with low nutrient concentrations ($1.0 \pm 0.2 \text{ d}^{-1}$) compared to a primary effluent with a higher nutrient load ($2.2 \pm 0.2 \text{ d}^{-1}$). In response to low phosphorus concentrations, microalgae have been shown to adjust their metabolic fluxes towards an efficient capture of extracellular phosphorus by: (i) stimulating the activity of phosphatases; (ii) producing high-affinity phosphorus transporters; or (iii) synthesising more transporters, which can explain the higher uptake rates (Su, 2021). Therefore, microalgae appear to respond to the low nutrient availability in the culture medium by quickly assimilating the limiting nutrient, which evidences their ability to adapt to different

Table 2
Gompertz model parameters for nitrogen and phosphorus.

N:P molar ratio	Nitrogen				Phosphorus			
	$k \text{ (d}^{-1}\text{)}$	$\lambda \text{ (d)}$	R^2	$RMSE \text{ (mg}_{\text{N}} \text{ L}^{-1}\text{)}$	$k \text{ (d}^{-1}\text{)}$	$\lambda \text{ (d)}$	R^2	$RMSE \text{ (mg}_{\text{P}} \text{ L}^{-1}\text{)}$
2	1.38 ± 0.08	0.82 ± 0.07	0.999	0.104	0.7 ± 0.1	0.7 ± 0.5	0.993	0.169
3	1.5 ± 0.1	0.7 ± 0.1	0.997	0.152	0.6 ± 0.1	0.7 ± 0.4	0.996	0.120
5	0.4 ± 0.2	1 ± 1	0.983	0.976	0.5 ± 0.2	0 ± 1	0.981	0.349
7	0.4 ± 0.2	0 ± 1	0.986	1.101	0.4 ± 0.2	0 ± 2	0.979	0.389
8	0.4 ± 0.1	1.1 ± 0.7	0.987	1.373	0.36 ± 0.06	0.3 ± 0.7	0.996	0.250
9	0.34 ± 0.08	1.6 ± 0.6	0.992	1.183	0.4 ± 0.1	1 ± 1	0.985	0.425
14	1.1 ± 0.2	1.4 ± 0.2	0.991	1.443	0.6 ± 0.1	0.0 ± 0.6	0.992	0.309
19	0.43 ± 0.07	1.0 ± 0.5	0.995	1.260	0.4 ± 0.1	0 ± 1	0.985	0.409
28	0.4 ± 0.2	0 ± 2	0.962	3.823	0.5 ± 0.2	0 ± 1	0.975	0.401
41	0.7 ± 0.1	1.4 ± 0.2	0.996	1.487	0.63 ± 0.08	0.3 ± 0.4	0.996	0.125
43	0.4 ± 0.1	0 ± 2	0.987	2.111	0.6 ± 0.2	0 ± 1	0.980	0.249
52	0.2 ± 0.2	0 ± 4	0.969	3.276	0.6 ± 0.1	1.7 ± 0.4	0.992	0.152
59	0.41 ± 0.07	2.4 ± 0.3	0.997	1.418	0.6 ± 0.1	0.2 ± 0.7	0.997	0.064
66	0.3 ± 0.2	0 ± 2	0.978	1.541	1.1 ± 0.1	1.4 ± 0.1	0.997	0.061
67	2 ± 11	2 ± 3	0.941	2.644	1.10 ± 0.07	1.04 ± 0.09	0.999	0.043

k : nutrient uptake rate; $RMSE$: root mean squared error; R^2 : coefficient of determination; λ : lag time.

environmental conditions.

3.3. GA-ANN models for biomass productivity and nutrient removal rates

Using the GAs, the optimal ANN hyperparameters were determined, such as the selected input variables, type of activation function, number of hidden neurons, and threshold variables and values. Table 3 presents the hyperparameters for the optimal ANNs for each output and corresponding performance indicators. Furthermore, a comparison between the experimental and predicted output values through ANN modelling is presented in Fig. 6. Regarding the ANN model for BP , high R^2 (0.951) and low $RMSE$ ($3.589 \text{ mg}_{\text{DW}} \text{ L}^{-1} \text{ d}^{-1}$) values were observed, representing a high fitting performance. Therefore, the ANN models efficiently described the time-course evolution of the output variables in various experiments, as presented in Fig. 7. Regardless of the regime, five out of the eight explanatory variables were selected: N_b , P_0 , P_b , t , and X_i . The variables $N:P_0$ and $N:P_i$ were not selected as input variables. This is in accordance with the previous analysis of the experimental data regarding microalgal growth, which showed that the average biomass productivities and specific growth rates were not impacted by the N:P ratio. X_i was identified as the threshold variable due to its great impact on biomass productivity. Microalgal growth can be divided into four key phases: lag, exponential, stationary, and death (Peter et al., 2022). As mentioned in Section 3.1., in the experimental conditions and duration of the present study, only two of these phases were observed for *C. vulgaris*: exponential and stationary. The first stage is characterised by an exponential increase in biomass concentration and, consequently, high biomass productivity. The latter phase occurs due to a decline in cell growth due to a limiting factor such as low nutrient availability. The growth rate balances this decline, leading to an approximately stable biomass concentration (Belaidi et al., 2020). Therefore, it is understandable that X_i would be the chosen variable to define the two regimes that describe biomass productivity.

The combined effect of each pair of input variables on the output variables was also analysed based on the determined ANN models. The 2D contour and 3D surface plots combining the effect of different input variables on each output are presented in Figures SM1-SM6 (Supplementary Materials). Regarding BP , for $X_i \leq 183.6 \text{ mg}_{\text{DW}} \text{ L}^{-1}$ (Fig. SM1), N_i and P_0 do not appear to have a high impact on biomass productivity when plotted with t and X_i . Furthermore, higher BP values were observed for lower t (1–3 d) and X_i , which correspond to the beginning of the experiment and to the exponential growth phase, in which biomass productivities are expected to be higher. Furthermore, P_i does not appear to affect the BP compared to t and low X_i values. Peaks in biomass productivity are observed when high P_0 and P_i or P_i and N_i are combined. Once again, the model appears to predict the real scenario, as high nutrient concentrations are observed at the beginning of the experiments, in which biomass productivities are higher due to the exponential microalgal growth. Furthermore, comparing the effect of P_0 and P_i on BP , higher values are predicted when P_i is approximately equal to P_0 , which once again corresponds to the initial stage of cultivation. A lower range of biomass productivities is predicted for X_i higher than 183.6

$\text{mg}_{\text{DW}} \text{ L}^{-1}$ (Fig. SM2), with an overall lower impact of the input variables. Nevertheless, higher BP is also described for a combination of lower values of X_i and t .

Regarding the ANN model for RR_N , R^2 and $RMSE$ values of 0.800 and $1.863 \text{ mg}_N \text{ L}^{-1} \text{ d}^{-1}$, respectively, were observed. Even though the coefficient of determination was lower compared to the one obtained for BP , the model provided a high fitting performance in several experiments, such as the one with an N:P molar ratio of 41 (Fig. 7 B). P_0 was selected as the threshold variable, which demonstrates the impact of this parameter on the RR_N , which is in accordance with the experimental observations from this study. For $P_0 \leq 8.06 \text{ mg}_P \text{ L}^{-1}$, the selected explanatory variables were N_b , P_0 , and X_i . Through the analysis of the surface plots (Fig. SM3), it is possible to observe that the combination of high X_i with high P_0 values maximises the RR_N . These results appear plausible since high biomass concentrations and phosphorus-replete conditions may allow a greater nitrogen uptake. However, when comparing the combined effect of N_i with P_0 and X_i , N_i revealed a greater impact on RR_N , with higher values maximising the output. Considering the results from the experiments with ratios 43 and 52, with identical phosphorus concentrations below the threshold value, higher N_0 (ratio 52) and consequently higher N_i available for consumption, also reflected an increase in the $RR_{N,\text{avg}}$. However, the ANN model predicts that for lower P_0 values, the RR_N slightly decreases, even with high N_b , which reflects the limiting role of phosphorus in nitrogen uptake. In the ANN model regime described for $P_0 > 8.06 \text{ mg}_P \text{ L}^{-1}$ (Fig SM4), $N:P_0$, P_i , t , and X_i were chosen as input variables. The only clear variable impact that maximised the RR_N was observed for low X_i values when plotted with $N:P_0$, P_i , and t . The initial stage of the experiments was characterised by low X_i values, high nutrient availability and high nutrient uptake to sustain the exponential growth, which can explain the higher nitrogen removal rates.

The ANN model described for RR_P provided R^2 and $RMSE$ values of 0.793 and $0.279 \text{ mg}_P \text{ L}^{-1} \text{ d}^{-1}$, respectively. High fitting performances were observed for various sets of experimental data, such as the one corresponding to an initial N:P ratio of 19 (Fig. 7 C). In this case, N_0 was selected as the threshold variable, which once again evidences the effect of the concentration of one nutrient on the removal of the other. As opposed to what was observed for the BP and RR_N models, the instantaneous biomass concentration does not appear to have an impact on RR_P , as it was not selected as an input variable. For $N_0 \leq 62.9 \text{ mg}_N \text{ L}^{-1}$ (Figure SM5), which corresponds to low N:P ratios, $N:P_0$, N_0 , N_b , P_b , and t were selected as input variables. The selection of both N_0 and N_i reflects the importance of nitrogen for phosphorus uptake, particularly for lower nitrogen concentrations. When comparing P_i with N_i , N_0 , and $N:P_0$, the first variable had a higher impact on RR_P , with higher values reflecting higher removal rates. Identically to what was observed for nitrogen, higher phosphorus availability (higher P_i) led to higher consumption rates. Nevertheless, a decrease in $N:P_0$ and N_0 for high P_i values reflected a slight decrease in the RR_P , evidencing the impact of nitrogen limitation on phosphorus uptake. Therefore, the maximum values were observed when high $N:P_0$ ratios and N_0 were combined with high P_b , as this reflects a situation under which microalgae still have high phosphorus levels to

Table 3
Hyperparameters for each artificial neural network and performance indicators.

Model	Activation function	Hidden neurons	R^2	$RMSE$
$BP = \begin{cases} ANN_1(N_i, P_0, P_i, t, X_i), & \text{if } X_i \leq 183.6 \\ ANN_2(N_i, P_0, P_i, t, X_i), & \text{if } X_i > 183.6 \end{cases}$	radbas tansig	6 5	0.951	$3.589 \text{ mg}_{\text{DW}} \text{ L}^{-1} \text{ d}^{-1}$
$RR_N = \begin{cases} ANN_1(N_i, P_0, X_i), & \text{if } P_0 \leq 8.06 \\ ANN_2(N : P_0, P_i, t, X_i), & \text{if } P_0 > 8.06 \end{cases}$	logsig tansig	8 8	0.800	$1.863 \text{ mg}_N \text{ L}^{-1} \text{ d}^{-1}$
$RR_P = \begin{cases} ANN_1(N : P_0, N_0, N_i, P_i, t), & \text{if } N_0 \leq 62.9 \\ ANN_2(N : P_0, N_i, P_0, P_i, t), & \text{if } N_0 > 62.9 \end{cases}$	tansig tansig	4 6	0.793	$0.279 \text{ mg}_P \text{ L}^{-1} \text{ d}^{-1}$

ANN_1 : Artificial neural network 1; ANN_2 : Artificial neural network 2; BP : biomass productivity ($\text{mg}_{\text{DW}} \text{ L}^{-1} \text{ d}^{-1}$); N_0 : initial nitrogen concentration ($\text{mg}_N \text{ L}^{-1}$); N_i : instantaneous nitrogen concentration ($\text{mg}_N \text{ L}^{-1}$); $N:P_0$: initial nitrogen to phosphorus molar ratio; P_0 : initial phosphorus concentration ($\text{mg}_P \text{ L}^{-1}$); P_i : instantaneous phosphorus concentration ($\text{mg}_P \text{ L}^{-1}$); $RMSE$: root mean squared error; RR_N : nitrogen removal rate ($\text{mg}_N \text{ L}^{-1} \text{ d}^{-1}$); RR_P : phosphorus removal rate ($\text{mg}_P \text{ L}^{-1} \text{ d}^{-1}$); R^2 : coefficient of determination; t : time; X_i : instantaneous biomass concentration ($\text{mg}_{\text{DW}} \text{ L}^{-1}$).

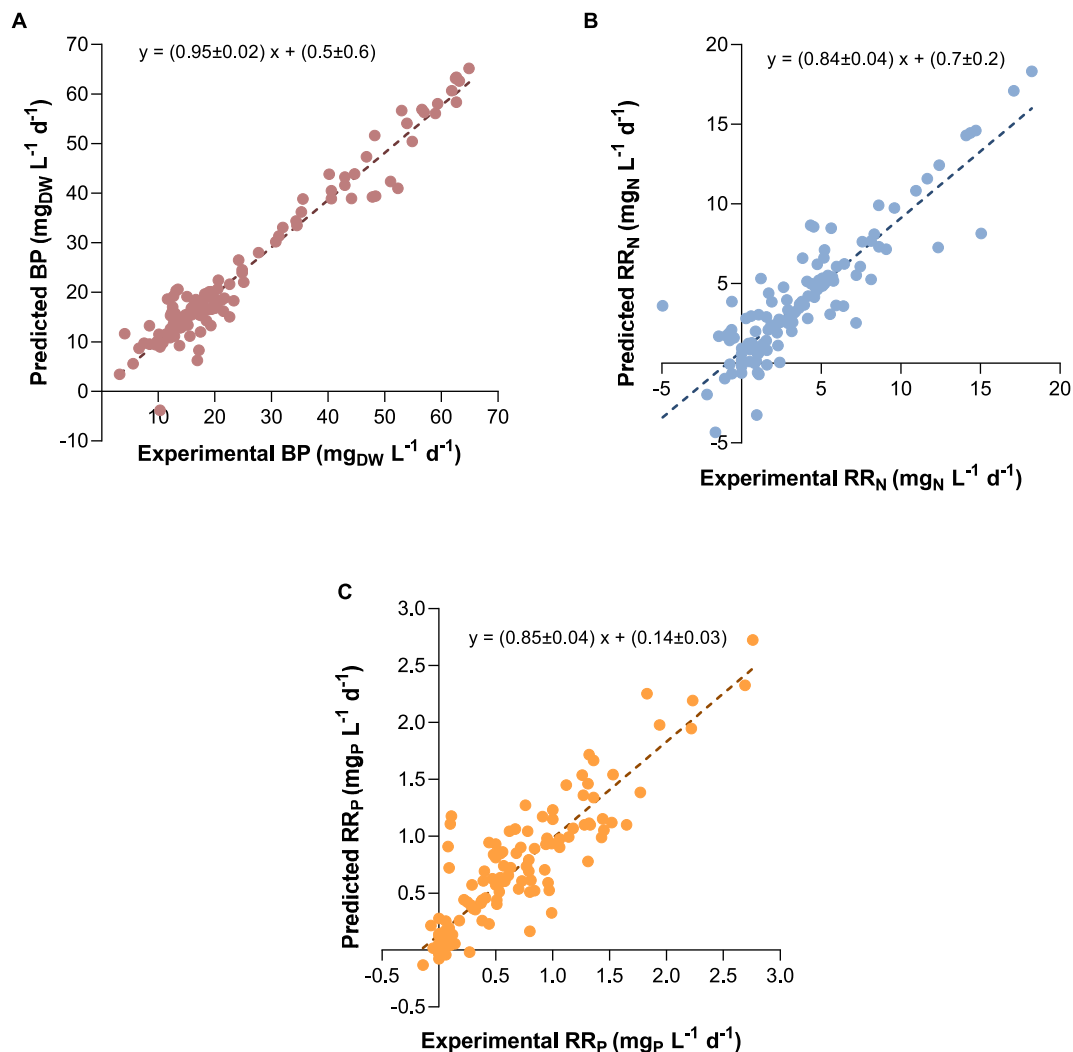


Fig. 6. Comparison between experimental and predicted values through ANN modelling for: (A) biomass productivity, BP ; (B) nitrogen removal rate, RR_N ; and (C) phosphorus removal rate, RR_P . The dashed lines correspond to the linear adjustment to the experimental data.

consume and an N:P proportion which allows that uptake. Regarding the regime for N_0 higher than $62.9 \text{ mg}_N \text{ L}^{-1}$, the selected explanatory variables were $N:P_0$, N_i , P_0 , P_i , and t . For this higher range of N_0 values, higher N:P ratios are observed, and nitrogen is no longer limiting phosphorus uptake. Therefore, phosphorus will be the main nutrient impacting its consumption, which is reflected in the choice of both P_i and P_0 as input variables. In fact, Fig. SM6 shows that P_i and P_0 have a higher impact on RR_P when plotted with N_i and t . In these plots, higher P_i leads to higher RR_P , as there is a high phosphorus content available to be consumed. However, extremely low P_0 showed higher removal rates, which can be explained by the high uptake rates described in Section 3.2 for high N:P ratios such as 66 and 67. In these conditions, due to the low available phosphorus at the beginning of cultivation, microalgae consumed this nutrient faster. Therefore, even though the average RR_P were lower due to the low P_0 , daily removal rates can be higher as a result of this quick consumption.

4. Conclusions

The results from this study demonstrated that *C. vulgaris* could easily adapt to different N:P molar ratios in synthetic wastewaters, achieving similar growth rates and biomass productivities, which is useful for maintaining the process's consistency when working with real

wastewaters. Furthermore, microalgae efficiently removed nitrogen and phosphorus from the wastewaters, with removal efficiencies/rates reaching $92.0 \pm 0.6\%/6.15 \pm 0.01 \text{ mg}_N \text{ L}^{-1} \text{ d}^{-1}$ for nitrogen and $98.2 \pm 0.2\%/0.92 \pm 0.03 \text{ mg}_P \text{ L}^{-1} \text{ d}^{-1}$ for phosphorus. Even though the different nitrogen and phosphorus concentrations used in this study did not limit microalgal growth, they had a significant impact on nutrient uptake. For instance, microalgal phosphorus uptake for low N:P ratios such as 2 and 3 was limited by nitrogen, while phosphorus limited nitrogen uptake with high ratios such as 66 and 67. Therefore, *C. vulgaris* most likely responded to the variations in the environmental conditions by altering its nutrient uptake fluxes and, consequently, the elemental biomass composition to maintain cellular growth. GA-ANN models for biomass productivity and nitrogen and phosphorus removal rates revealed a high fitting performance, with R^2 of 0.951, 0.800, and 0.793, respectively. The models effectively described the variation of these parameters with different input variables, and the conclusions were in accordance with the experimental findings. For biomass productivity, the initial biomass concentration was selected as the threshold variable, since this is the variable that distinguishes between two productivity regimes: one during the exponential growth phase and the other during the stationary phase. For nitrogen and phosphorus removal rates, the threshold variables were the initial concentrations of phosphorus and nitrogen, respectively. These results also reflect the great impact that the

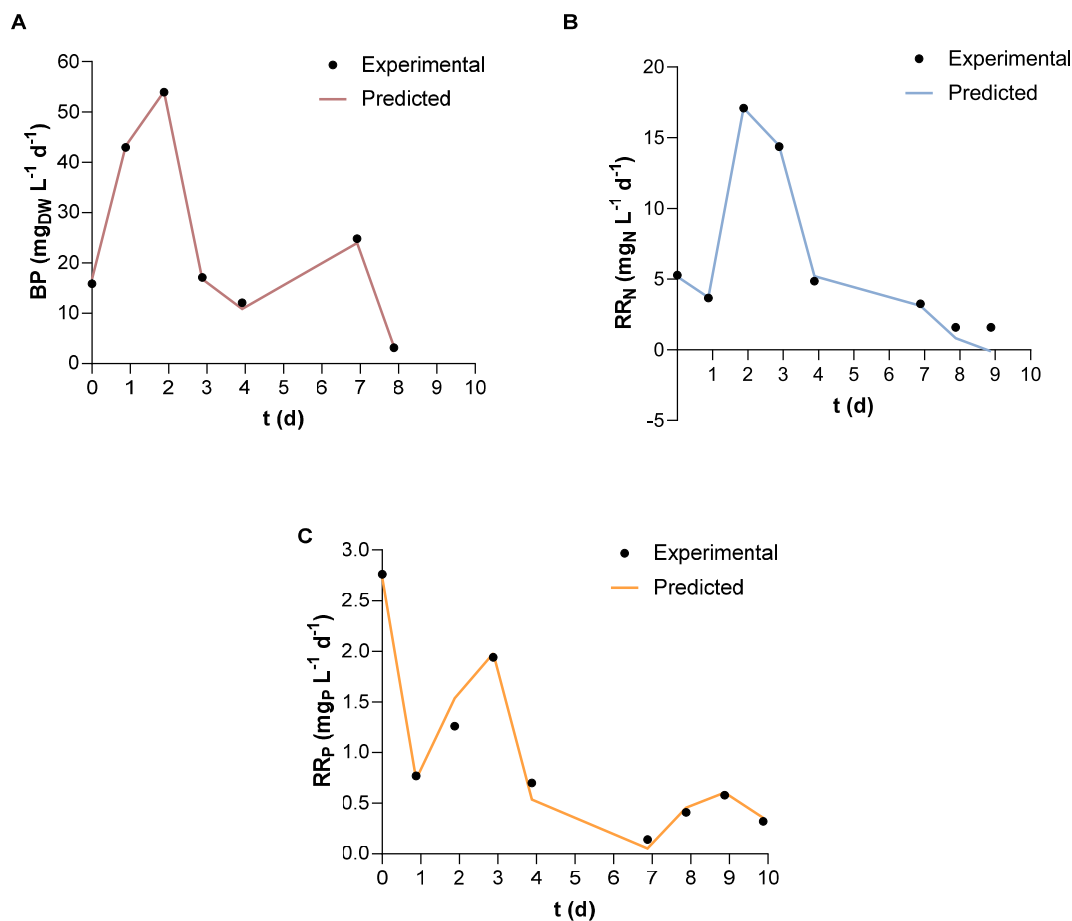


Fig. 7. Comparison between the time-course evolution of experimental and predicted values through ANN modelling for: (A) biomass productivity, BP , corresponding to an N:P molar ratio of 3; (B) nitrogen removal rate, RR_N , corresponding to an N:P molar ratio of 41; and (C) phosphorus removal rate, RR_P , corresponding to an N:P molar ratio of 19.

concentration of one nutrient has on the removal of the other. In conclusion, the present study indicates that microalgae-based systems can be an efficient, reliable, and sustainable technology for wastewater treatment and GA-ANN models can be a relevant tool for modelling and control of microalgal systems.

Credit roles

José C. M. Pires, Ana L. Gonçalves: **Conceptualization**; José C. M. Pires, Eva Salgado: **Formal analysis**; José C. M. Pires: **Funding acquisition**; Ana L. Gonçalves, Eva M. Salgado, Ana F. Esteves: **Investigation**; Ana L. Gonçalves, Eva M. Salgado, Ana F. Esteves, José C. M. Pires: **Methodology**; José C. M. Pires: **Project administration**; José C. M. Pires: **Resources**; José C. M. Pires, Eva M. Salgado: **Software**; José C. M. Pires, Ana L. Gonçalves: **Supervision**; Eva M. Salgado, José C. M. Pires: **Visualization**; Eva M. Salgado: **Writing-Original Draft Preparation**; Ana F. Esteves, Ana L. Gonçalves, José C. M. Pires: **Writing – Reviewing and Editing**.

Funding

This work was financially supported by: (i) LA/P/0045/2020 Associate Laboratory in Chemical Engineering, University of Porto, Portugal (ALiCE), UIDB/00511/2020- UIDP/00511/2020 Laboratory for Process Engineering, Environment, Biotechnology and Energy, Faculty of

Engineering, University of Porto, Portugal (LEPABE) and UIDB/50020/2020-UIDP/50020/2020 Laboratory of Separation and Reaction Engineering - Laboratory of Catalysis and Materials, Faculty of Engineering, University of Porto, Portugal (Associate Laboratory LSRE- LCM) funded by national funds through Fundação Para a Ciência e Tecnologia/Ministério da Ciência, Tecnologia e Ensino Superior FCT/MCTES (PIDDAC); and (ii) Project PhotoBioValue (ref. PTDC/BTA-BTA/2902/2021), funded by FEDER funds through COMPETE2020-Programa Operacional Competitividade e Internacionalização (POCI) and by national funds (PIDDAC) through FCT/MCTES. A.F. Esteves and E.M. Salgado thank FCT for the financial support of their work through the FCT PhD Research Scholarships 2020.05477.BD and 2021.07412.BD, respectively.

Declaration of competing interest

The authors declare that they have no known competing financial interests or personal relationships that could have appeared to influence the work reported in this paper

Data availability

Data will be made available on request.

Appendix A. Supplementary data

Supplementary data to this article can be found online at <https://doi.org/10.1016/j.envres.2023.116076>.

References

- Afonso, N.F., Pires, J.C., 2017. Characterization of surface ozone behavior at different regimes. *Appl. Sci.* 7, 944.
- Ahmed, S.F., Mofijur, M., Parisa, T.A., Islam, N., Kusumo, F., Inayat, A., Badruddin, I.A., Khan, T.Y., Ong, H.C., 2022. Progress and challenges of contaminate removal from wastewater using microalgae biomass. *Chemosphere* 286, 131656.
- Alketife, A.M., Judd, S., Znad, H., 2017. Synergistic effects and optimization of nitrogen and phosphorus concentrations on the growth and nutrient uptake of a freshwater *Chlorella vulgaris*. *Environ. Technol.* 38, 94–102.
- APHA, 2017. Standard Methods for the Examination of Water and Wastewater. American Public Health Association, Washington, D.C., United States of America.
- Arranz, A., Bordel, S., Villaverde, S., Zamarréno, J., Guieysse, B., Munoz, R., 2008. Modeling photosynthetically oxygenated biodegradation processes using artificial neural networks. *J. Hazard Mater.* 155, 51–57.
- Bahramian, M., Dereli, R.K., Zhao, W., Giberti, M., Casey, E., 2023. Data to intelligence: the role of data-driven models in wastewater treatment. *Expert Syst. Appl.*, 119453.
- Behl, K., Seshacharan, P., Joshi, M., Sharma, M., Mathur, A., Kareya, M.S., Jutur, P.P., Bhatnagar, A., Nigam, S., 2020. Multifaceted applications of isolated microalgae *Chlamydomonas sp. TRC-1* in wastewater remediation, lipid production and bioelectricity generation. *Bioresour. Technol.* 304, 122993.
- Belaïdi, F.S., Salvagnac, L., Souleille, S.A., Blatché, M.-C., Bedel-Pereira, E., Séguin, I., Temple-Boyer, P., Launay, J., 2020. Accurate physiological monitoring using lab-on-a-chip platform for aquatic micro-organisms growth and optimized culture. *Sens. Actuators. B Chem.* 321, 128492.
- Braun, J.C., Colla, L.M., 2022. Use of microalgae for the development of biofertilizers and biostimulants. *Bioenergy Res* 1–22.
- Carvalho, Y.O., Oliveira, W.V., Pagano, R.L., Silva, C.F., 2021. Application of artificial neural networks in the tertiary treatment of liquid effluent with the microalgae *Chlorella vulgaris*. *Chem. Eng. Technol.* 44, 1863–1869.
- Chai, W.S., Tan, W.G., Munawaroh, H.S.H., Gupta, V.K., Ho, S.-H., Show, P.L., 2021. Multifaceted roles of microalgae in the application of wastewater biotreatment: a review. *Environ. Pollut.* 269, 116236.
- Chen, C.-Y., Kuo, E.-W., Nagarajan, D., Ho, S.-H., Dong, C.-D., Lee, D.-J., Chang, J.-S., 2020. Cultivating *Chlorella sorokiniana* AK-1 with swine wastewater for simultaneous wastewater treatment and algal biomass production. *Bioresour. Technol.* 302, 122814.
- Cheng, T., Wei, C.-H., Leiknes, T., 2017. Polishing of anaerobic secondary effluent by *Chlorella vulgaris* under low light intensity. *Bioresour. Technol.* 241, 360–368.
- Choi, H.J., Lee, S.M., 2015. Effect of the N/P ratio on biomass productivity and nutrient removal from municipal wastewater. *Bioproc. Biosyst. Eng.* 38, 761–766.
- Chu, R., Hu, D., Zhu, L., Li, S., Yin, Z., Yu, Y., 2022. Recycling spent water from microalgae harvesting by fungal pellets to re-cultivate *Chlorella vulgaris* under different nutrient loads for biodiesel production. *Bioresour. Technol.* 344, 126227.
- Cordoba-Perez, M., Lasa, H., 2021. CO₂-Derived carbon capture using microalgae and sodium bicarbonate in a PhotoBioCREC unit: kinetic modeling. *Processes* 9, 1296.
- Escapa, C., Coimbra, R., Paniagua, S., García, A., Otero, M., 2017. Comparison of the culture and harvesting of *Chlorella vulgaris* and *Tetradismus obliquus* for the removal of pharmaceuticals from water. *J. Appl. Phycol.* 29, 1179–1193.
- Fard, M.B., Mirbagheri, S.A., Pendashteh, A., Alavi, J., 2020. Estimation of effluent parameters of slaughterhouse wastewater treatment with artificial neural network and B-spline quasi interpolation. *Int. J. Environ. Res.* 14, 527–539.
- Fernandes, T., Fernandes, I., Andrade, C.A.P., Cordeiro, N., 2020. Assessing the impact of sulfur concentrations on growth and biochemical composition of three marine microalgae. *J. Appl. Phycol.* 32, 967–975.
- Ganeshkumara, V., Subashchandrabose, S.R., Dharmarajan, R., Venkateswarlud, K., Naidub, R., Megharaj, M., 2018. Use of mixed wastewaters from piggery and winery for nutrient removal and lipid production by *Chlorella sp. MM3*. *Bioresour. Technol.* 256, 254–258.
- Gil-Izquierdo, A., Pedreño, M., Montoro-García, S., Tárraga-Martínez, M., Iglesias, P., Ferreres, F., Barceló, D., Núñez-Delgado, E., Gabaldón, J., 2021. A sustainable approach by using microalgae to minimize the eutrophication process of Mar Menor lagoon. *Sci. Total Environ.* 758, 143613.
- Gonçalves, A.L., Pires, J.C., Simões, M., 2016. Wastewater polishing by consortia of *Chlorella vulgaris* and activated sludge native bacteria. *J. Clean. Prod.* 133, 348–357.
- Gonçalves, A.L., Pires, J.C., Simões, M., 2017. A review on the use of microalgal consortia for wastewater treatment. *Algal Res.* 24, 403–415.
- Gramegna, G., Scortica, A., Scafati, V., Ferella, F., Gurrieri, L., Giovannoni, M., Bassi, R., Sparla, F., Mattei, B., Benedetti, M., 2020. Exploring the potential of microalgae in the recycling of dairy wastes. *Bioresour. Technol.* 12, 100604.
- Han, W., Jin, W., Li, Z., Wei, Y., He, Z., Chen, C., Qin, C., Chen, Y., Tu, R., Zhou, X., 2021. Cultivation of microalgae for lipid production using municipal wastewater. *Process Saf. Environ. Protect.* 155, 155–165.
- Hemalathaa, M., Sravana, J.S., Minc, B., Mohan, S.V., 2019. Microalgae-biorefinery with cascading resource recovery design associated to dairy wastewater treatment. *Bioresour. Technol.* 284, 424–429.
- Hossain, S.Z., Sultana, N., Jassim, M.S., Coskuner, G., Hazin, L.M., Razzak, S.A., Hossain, M.M., 2022. Soft-computing modeling and multiresponse optimization for nutrient removal process from municipal wastewater using microalgae. *J. Water Process Eng.* 45, 102490.
- Jana, D.K., Bhunia, P., Adhikary, S.D., Bej, B., 2022. Optimization of effluents using artificial neural network and support vector regression in detergent industrial wastewater treatment. *Cleaner Chem. Eng.* 3, 100039.
- Japar, A.S., Takriff, M.S., Yasin, N.H.M., 2021. Microalgae acclimatization in industrial wastewater and its effect on growth and primary metabolite composition. *Algal Res.* 53, 102163.
- Javed, F., Rehman, F., Khan, A.U., Fazal, T., Hafeez, A., Rashid, N., 2022. Real textile industrial wastewater treatment and biodiesel production using microalgae. *Biomass Bioenergy* 165, 106559.
- Jawad, J., Hawari, A.H., Zaidi, S.J., 2021. Artificial neural network modeling of wastewater treatment and desalination using membrane processes: a review. *Chem. Eng. J.* 419, 129540.
- Katoch, S., Chauhan, S.S., Kumar, V., 2021. A review on genetic algorithm: past, present, and future. *Multimed. Tool. Appl.* 80, 8091–8126.
- Kröger, M., Klemm, M., Nelles, M., 2018. Hydrothermal disintegration and extraction of different microalgae species. *Energies* 11, 450.
- Lee, B.-H., Park, S.-Y., Heo, Y.-S., Yea, S.-S., Kim, D.-E., 2009. Efficient colorimetric assay of RNA polymerase activity using inorganic pyrophosphatase and ammonium molybdate. *Bull. Kor. Chem. Soc.* 30, 2485–2488.
- Leong, W.H., Kiatkittipong, W., Lam, M.K., Khoo, K.S., Show, P.L., Mohamad, M., Chong, S., Abdurrahman, M., Lim, J.W., 2022. Dual nutrient heterogeneity modes in a continuous flow photobioreactor for optimum nitrogen assimilation to produce microalgal biodiesel. *Renew. Energy* 184, 443–451.
- Li, J., Qian, J., Tang, J., Jin, Z., Lu, Q., Cheng, J., Zhou, X., Zhang, X., Fu, S., Wan, T., 2022. Enhancement of ammonium removal from landfill leachate using microalgae by an integrated strategy of nutrient balance and trophic mode conversion. *Algal Res.* 61, 102572.
- Li, K., Liu, Q., Fang, F., Luo, R., Lu, Q., Zhou, W., Huo, S., Cheng, P., Liu, J., Addy, M., 2019. Microalgae-based wastewater treatment for nutrients recovery: a review. *Bioresour. Technol.* 291, 121934.
- Liyanaarachchi, V.C., Nishshanka, G.K.S.H., Nimarshana, P.H.V., Ariyadasa, T.U., Attalage, R.A., 2020. Development of an artificial neural network model to simulate the growth of microalga *Chlorella vulgaris* incorporating the effect of micronutrients. *J. Biotechnol.* 312, 44–55.
- Lucakova, S., Branyikova, I., Hayes, M., 2022. Microalgal proteins and bioactives for food, feed, and other applications. *Appl. Sci.* 12, 4402.
- Lv, J., Feng, J., Liu, Q., Xie, S., 2017. Microalgal cultivation in secondary effluent: recent developments and future work. *Int. J. Mol. Sci.* 18, 79.
- Mirjalili, S., Song Dong, J., Sadiq, A.S., Faris, H., 2020. Genetic algorithm: theory, literature review, and application in image reconstruction. In: Mirjalili, S., et al. (Eds.), *Nature-Inspired Optimizers: Theories, Literature Reviews and Applications*. Springer Nature, Switzerland, pp. 69–85.
- Mohsenpour, S.F., Hennige, S., Willoughby, N., Adeloje, A., Gutierrez, T., 2021. Integrating micro-algae into wastewater treatment: a review. *Sci. Total Environ.* 752, 142168.
- Moral, H., Aksoy, A., Gokcay, C.F., 2008. Modeling of the activated sludge process by using artificial neural networks with automated architecture screening. *Comput. Chem. Eng.* 32, 2471–2478.
- Peter, A.P., Koyande, A.K., Chew, K.W., Ho, S.-H., Chen, W.-H., Chang, J.-S., Krishnamoorthy, R., Banat, F., Show, P.L., 2022. Continuous cultivation of microalgae in photobioreactors as a source of renewable energy: current status and future challenges. *Renewable Sustainable Energy Rev.* 154, 111852.
- Raheem, A., Sivasangar, S., Azlina, W.W., Yap, Y.T., Danquah, M.K., Harun, R., 2015. Thermogravimetric study of *Chlorella vulgaris* for syngas production. *Algal Res.* 12, 52–59.
- Sakiewicz, P., Piotrowski, K., Ober, J., Karwot, J., 2020. Innovative artificial neural network approach for integrated biogas-wastewater treatment system modelling: effect of plant operating parameters on process intensification. *Renewable Sustainable Energy Rev.* 124, 109784.
- Salgado, E.M., Gonçalves, A.L., Sánchez-Soberón, F., Ratola, N., Pires, J.C., 2022. Microalgal cultures for the bioremediation of urban wastewaters in the presence of siloxanes. *Int. J. Environ. Res. Publ. Health* 19, 2634.
- Salgado, E.M., Pires, J.C., 2023. Photobioreactors modeling and simulation - photobioreactors: design and applications. In: Sirohi, R., et al. (Eds.), *Current Developments in Biotechnology and Bioengineering*. Elsevier Science & Technology, pp. 89–120.
- Silva, M.L., Gonçalves, A.L., Vilar, V.J.P., Pires, J.C.M., 2021. Experimental and techno-economic study on the use of microalgae for paper industry effluents remediation. *Sustainability* 13, 1314.
- Silva, N., Gonçalves, A., Moreira, F., Silva, T., Martins, F., Alvim-Ferraz, M., Boaventura, R., Vilar, V., Pires, J., 2015. Towards sustainable microalgal biomass production by phycoremediation of a synthetic wastewater: a kinetic study. *Algal Res.* 11, 350–358.
- Su, Y., 2021. Revisiting carbon, nitrogen, and phosphorus metabolisms in microalgae for wastewater treatment. *Sci. Total Environ.* 762, 144590.
- Suteja, Y., Dirgayusa, I.G.N.P., Cordova, M.R., Rachman, A., Rintaka, W.E., Takarina, N. D., Putri, W.A.E., Purwiyanto, A.I.S., 2021. Identification of potentially harmful microalgal species and eutrophication status update in Benoa Bay, Bali, Indonesia. *Ocean Coast Manag.* 210, 105698.
- Sutherland, D.L., Ralph, P.J., 2019. Microalgal bioremediation of emerging contaminants-Opportunities and challenges. *Water Res.* 164, 114921.
- Tao, R., Kinnunen, V., Praveenkumar, R., Lakanieni, A.-M., Rintala, J.A., 2017. Comparison of *Scenedesmus acuminatus* and *Chlorella vulgaris* cultivation in liquid

- digestates from anaerobic digestion of pulp and paper industry and municipal wastewater treatment sludge. *J. Appl. Phycol.* 29, 2845–2856.
- Tran, D.T., Nguyen, H.Y., Van Do, T.C., Show, P.L., Le, T.G., 2020. Factors affecting pollutants removal and biomass production capability of *Chlorella variabilis TH03* in domestic wastewater. *Mater. Sci. Energy Technol.* 3, 545–558.
- Umdu, E., 2020. Univ, Y., Building integrated photobioreactor. In: Pacheco-Torgal, F., et al. (Eds.), *Bio-Based Materials and Biotechnologies for Eco-Efficient Construction*. Woodhead Publishing, Sawston, UK, pp. 243–258.
- Vale, M.A., Ferreira, A., Pires, J.C.M., Gonçalves, A.L., 2020. CO₂ capture using microalgae. In: Rahimpour, M.R., et al. (Eds.), *Advances in Carbon Capture: Methods, Technologies and Applications*. Woodhead Publishing, Sawston, United Kingdom, pp. 381–405.
- Wang, G., Jia, Q.-S., Zhou, M., Bi, J., Qiao, J., Abusorrah, A., 2022. Artificial neural networks for water quality soft-sensing in wastewater treatment: a review. *Artif. Intell. Rev.* 55, 565–587.
- Whitton, R., Ometto, F., Pidou, M., Jarvis, P., Villa, R., Jefferson, B., 2015. Microalgae for municipal wastewater nutrient remediation: mechanisms, reactors and outlook for tertiary treatment. *Environ. Technol. Rev.* 4, 133–148.
- Yaakob, M.A., Mohamed, R.M.S.R., Al-Gheethi, A., Aswathnarayana Gokare, R., Ambati, R.R., 2021. Influence of nitrogen and phosphorus on microalgal growth, biomass, lipid, and fatty acid production: an overview. *Cells* 10, 393.
- Zhang, Q., Yu, H., Barbiero, M., Wang, B., Gu, M., 2019. Artificial neural networks enabled by nanophotonics. *Light Sci. Appl.* 8, 42.